J. Fluid Mech. (1983), *vol.* 127, *pp.* 341–352
Printed in Great Britain

Boundary-layer transition on a rotating cone in axial flow

By R. KOBAYASHI, Y. KOHAMA
Institute of High Speed Mechanics, Tohoku University, Sendai, Japan

AND M. KUROSAWA
Turbine Engineering Department, Mitsubishi Heavy Industries Ltd, Tokyo, Japan

(Received 25 January 1982 and in revised form 8 September 1982)

The purpose of the present paper is to investigate the structure of the laminar–turbulent transition region for the three-dimensional boundary layer along a 30° cone rotating in external axial flow. Spiral vortices, which were assumed as small disturbances in the present stability analysis, are observed experimentally in the transition region. The process of transition to a turbulent boundary layer is visualized in detail. When the ratio of rotational speed to external axial flow is increased, the critical and transition Reynolds numbers decrease remarkably. The spiral angle and the number of vortices appearing on the cone decrease as the rotational speed ratio is increased.

1. Introduction

A detailed study of laminar–turbulent transition in the boundary layer along a cone rotating in axial flow contributes to the understanding of the basic mechanism in transition regions of complex three-dimensional boundary layers on rotating axisymmetric bodies and also in internal flows of turbomachines, because in the case of rotating cones one can investigate changes in the boundary-layer characteristics caused by the rotational motion by using a small number of geometrical and mechanical parameters. Although previous studies of rotating cones were carried out for boundary layers with heat and mass transfer (Illingworth 1953; Salzberg & Kezios 1965; Tien & Tsuji 1965; Koh & Price 1967) and for those in still fluid (Tien & Campbell 1963; Kreith 1966; Kappesser, Greif & Cornet 1973; Koosinlin, Launder & Sharma 1974), the mechanism of the transition phenomenon has not been clarified. Only a transition region on a rotating disk in still fluid has been studied in detail (see e.g. Gregory, Stuart & Walker 1955; Chin & Litt 1972; Kobayashi, Kohama & Takamadate 1980). Recently Mueller *et al.* (1981) observed a transition region on a cylindrical body rotating in an axial flow. In the case of rotating cones, centrifugal instability must play an important role in the transition phenomenon.

The purpose of the present paper is to clarify experimentally the structure of the transition region for an incompressible boundary layer along a cone rotating in axial flow. The cone has a total included angle of 30°, as shown in figure 1, where the rotation is expected to have a remarkable effect upon the transition phenomenon. The experiment is compared with a theoretical analysis obtained numerically on the basis of the linear stability theory of Kobayashi (1981).

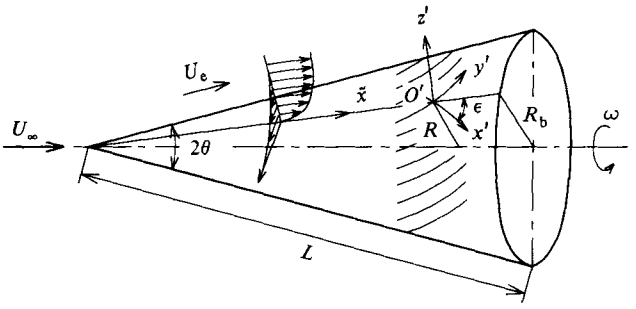

FIGURE 1. Rotating cone in axial flow and coordinate system.

2. Theoretical analysis

In the linear stability theory, small perturbations were assumed to be of spiral vortices. The origin O' of an orthogonal curvilinear coordinate system (x', y', z') is fixed on the surface of the rotating cone, as seen in figure 1, and the y' axis is chosen to coincide with the vortex axis, so that the x' axis makes an angle ϵ to the meridian of the cone. The velocity perturbations were written in vector form as $\mathbf{v}' = \hat{\mathbf{v}}(z') \exp i(\alpha x' - \lambda t)$. The wavenumber α in the x' direction is real and λ is complex, with the real part λ_r related to the phase velocity λ_r/α and the imaginary part λ_i being the amplification rate; t is the time. A set of perturbation equations governing the instability and a numerical procedure for solving the eigenvalue problem were then given. From these equations it can be seen that a significant parameter governing the present phenomenon is the local rotational speed ratio S $(= \omega R/U_e)$, which is defined as the ratio of the local circumferential velocity ωR at the cone surface to the local flow velocity U_e at the outer edge of the boundary layer, where ω denotes the angular speed of the cone, and R the local radial distance from the axis of symmetry. The predicted direction of the spiral-vortex axis, which makes an angle ϵ to the circumferential direction, was determined under the condition that the amplification of the perturbations is a maximum. The perturbations then propagate at an angle ϵ relative to the meridian of the cone. A numerical example was shown for a 30° cone at the local rotational speed ratio $S = 3$.

Because S varies along the cone surface, additional numerical analyses were made at $S = 1{\cdot}5$ and 2 on the basis of the linear stability theory mentioned above. The results are given in table 1. The displacement thickness δ_1 of the laminar boundary layer and the momentum thickness δ_2, calculated from the meridional component of the velocity field, are given by using the following dimensionless expressions:

$$\bar{\delta}_1 = \delta_1 \left(\frac{U_e}{\nu R}\right)^{\frac{1}{2}}, \quad \bar{\delta}_2 = \delta_2 \left(\frac{U_e}{\nu R}\right)^{\frac{1}{2}}, \tag{1}$$

where R is the local radial distance from the axis of symmetry and ν is the kinematic viscosity of the fluid. $H(= \delta_1/\delta_2)$ is the shape parameter. The Reynolds number Re_x is defined as $Re_x = U_e \tilde{x}/\nu$, where $\tilde{x}$ is the distance from the apex of the cone along the meridian. The critical Reynolds number $Re_{x,c}$ is the minimum value of Re_x in the state of neutral stability, and $Re_{x,m}$ gives a state in which the amplification rate of perturbations becomes maximum for the angle ϵ given in table 1. The dimensionless wavenumber σ is defined as $\sigma = \alpha\delta_1 \sin\theta$ using the wavenumber α in the x' direction, and σ_c and σ_m are the wavenumbers associated with the Reynolds numbers $Re_{x,c}$ and $Re_{x,m}$ respectively.

S	$\bar{\delta}_1$	$\bar{\delta}_2$	H	ϵ	$Re_{x,c}$	$Re_{x,m}$	σ_c	σ_m
1·5	1·442	0·665	2·17	30·2°	$1{\cdot}21 \times 10^3$	$4{\cdot}94 \times 10^4$	0·75	1·60
2	1·225	0·608	2·01	22·5°	$8{\cdot}35 \times 10^2$	$2{\cdot}84 \times 10^4$	0·75	1·48
3	0·819	0·454	1·81	13·6°	$5{\cdot}21 \times 10^2$	$1{\cdot}12 \times 10^4$	0·63	1·10

TABLE 1. Numerical data for laminar boundary layer on a 30° cone rotating in axial flow and its stability analysis in relation to rotational speed ratio S

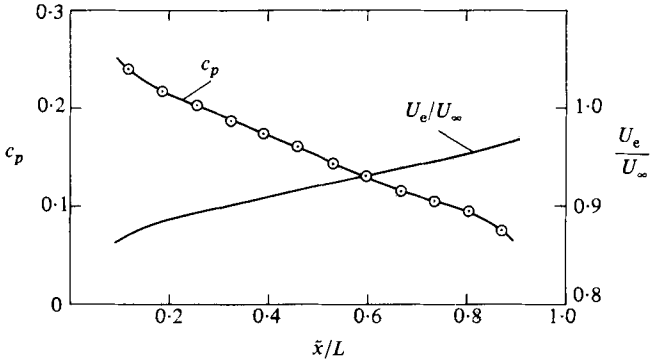

FIGURE 2. Distributions of pressure coefficient c_p and velocity U_e/U_∞ at outer edge of boundary layer.

3. Experiments

3.1. *Apparatus and procedure*

We used a low-turbulence wind tunnel (Ito *et al.* 1980) of the Laboratory for Air-Flow Measurements in the Institute of High Speed Mechanics, Tohoku University. The test section was set in a state of open-jet type, 508 mm long. The shape of the contraction exit is a regular octagon of subtense length 293 mm. The test cone (figure 1) had total angle $2\theta = 30°$, and base diameter $2R_b = 89{\cdot}2$ mm and generation-line length $L = 172{\cdot}7$ mm; it was made of aluminium alloy, and its surface was finished smooth. The cone was mounted horizontally in the test section of the wind tunnel and was driven by a d.c. motor through a V-belt. The rotating speed can be controlled continuously up to 3400 r.p.m. The turbulence intensities $(\overline{u'^2})^{\frac{1}{2}}/U_\infty$ of the wind tunnel were 0·05–0·15 % for wind speed U_∞ of 1–14 m/s in a state where the test cone was set in the test section; here u' denotes the longitudinal velocity fluctuations at a position 58 mm downstream from the centre of the contraction exit.

A hot-wire anemometer was used to measure the velocity field. In order to determine the direction of the spiral vortices appearing in the transition region, we used a parallel probe of two hot wires separated by 4·2 mm, which could be rotated around the z' axis through a range of 180°. We decided the angle ϵ of the spiral vortices by measuring the direction in which periodical signals obtained from the two hot wires were in the same phase. Flow patterns in the transition region were visualized by spreading titanium tetrachloride on the surface of another black-painted 30° cone, which was 198·5 mm in base diameter and was set in another 600 mm × 600 mm open-circuit wind tunnel.

Figure 2 shows distributions of the surface pressure c_p and the flow velocity U_e at the outer edge of the boundary layer along the surface of the test cone. The surface

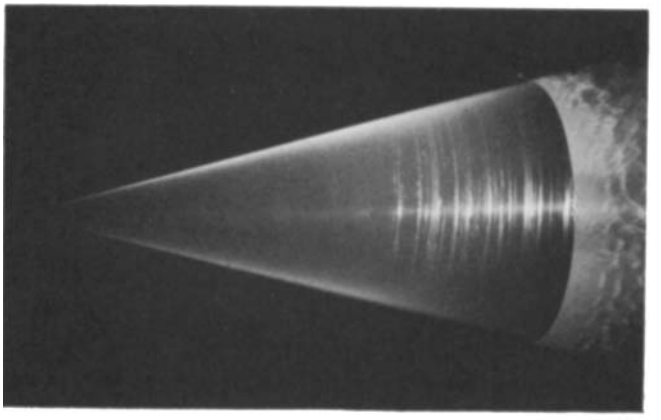

(*a*)

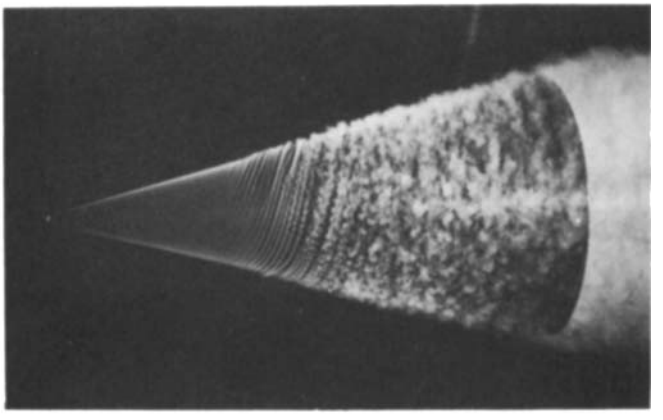

(*b*)

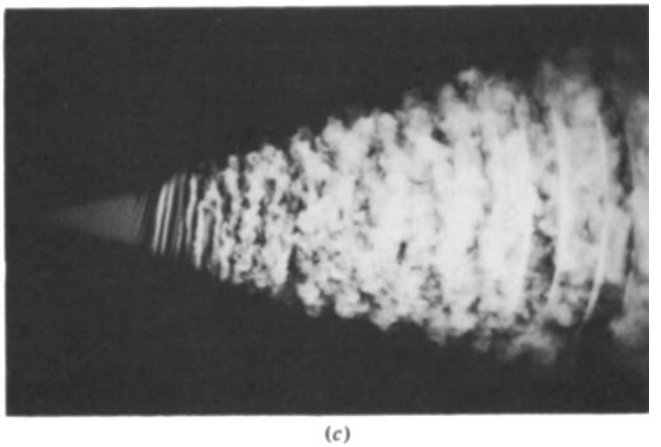

(*c*)

FIGURE 3. Flow visualization of boundary layer on rotating cone in axial flow: (*a*) $U_\infty = 2{\cdot}05$ m/s, $N = 300$ r.p.m.; (*b*) 1·7 m/s, 670 r.p.m.; (*c*) 1·0 m/s, 1200 r.p.m.

FIGURE 4. Cross-sectional observation of spiral vortices; $U_\infty = 1{\cdot}7$ m/s, $N = 670$ r.p.m.

pressure p was measured in the non-rotating state. The pressure coefficient c_p is defined as $c_p = 2(p-p_\infty)/\rho U_\infty^2$, where p_∞ is the upstream pressure and U_∞ is the approaching-flow velocity. As Okamoto, Yagita & Kamijima (1976) verified, the surface pressure is not affected by rotation of the cone. The flow velocity U_e was calculated by the measured pressure coefficient c_p using Bernoulli's equation.

3.2. *Flow visualizations of transition region*

The photographs in figure 3 show flow patterns of the boundary-layer flow on the rotating cone. In these photographs a uniform flow is given from the left, and the rotation vector of the cone is in the right direction of the rotation axis as shown in figure 1. Figure 3 (*a*) represents the flow condition in which the cone surface is covered wholly with the laminar boundary layer, where circumferential streaks on the cone surface are from the titanium tetrachloride spread on the whole surface. In figure 3 (*b*) one can see regular spiral vortices in the transition region between the laminar boundary layer on the left and the turbulent boundary layer on the right. As shown in figure 3 (*c*), the position of the transition region shifts in the direction of the cone apex as the rotation speed N of the cone is increased further. In figure 4, cross-sections of the spiral vortices are made visible by a sheet of light along the meridian of the rotating cone. In the linear stability theory we assumed disturbances of spiral vortex type by analogy with the rotating-disk problem (Kobayashi *et al.* 1980). Figures 3 and 4 show that the assumption for the disturbances in the stability theory is reasonable. Figure 5 is a close-up photograph of the spiral vortices near to the turbulent region, in which one can find the second instability appearing regularly along the spiral-vortex axes and a transition process from the regular flow pattern to the turbulent flow.

3.3. *Critical and transition Reynolds numbers*

Experimental results for the critical Reynolds number $Re_{x,c}$ and the transition Reynolds number $Re_{x,t}$ are shown in figure 6; they were measured under various conditions of the approaching-flow velocity ($U_\infty = 0{\cdot}76$–$13{\cdot}52$ m/s) and the rotation

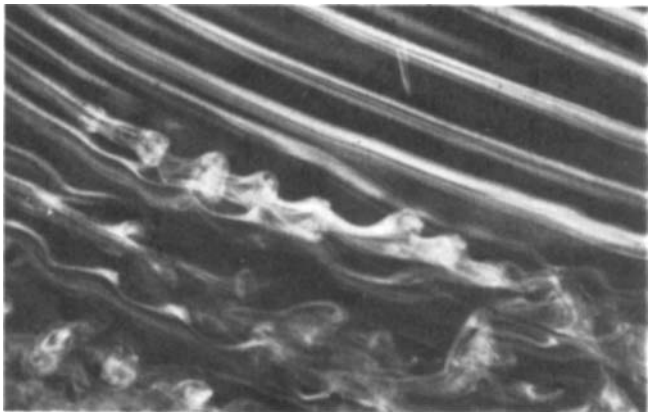

FIGURE 5. Transition process from spiral vortices to turbulent state; $U_\infty = 2{\cdot}9$ m/s, $N = 700$ r.p.m., direction of rotation from right to left.

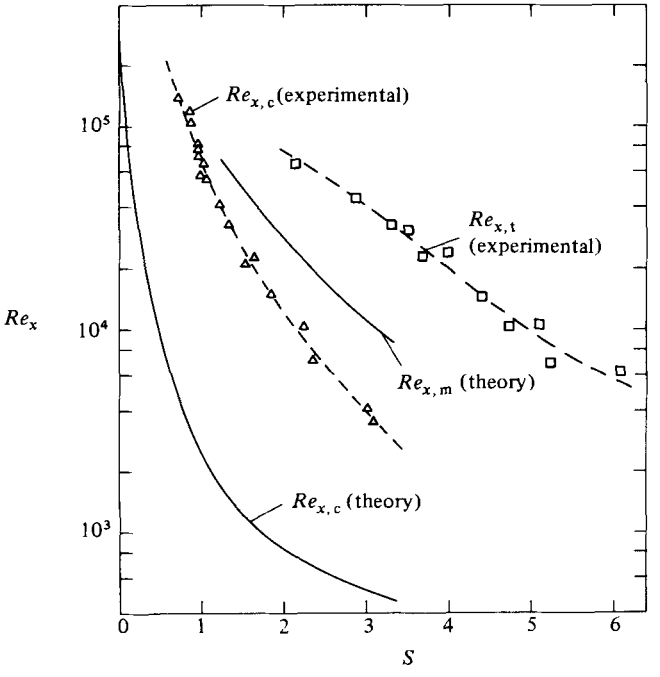

FIGURE 6. Critical Reynolds number $Re_{x,c}$ and transition Reynolds number $Re_{x,t}$.

speed ($N = 1119$–3230 r.p.m.). The solid lines represent the theoretical values of $Re_{x,c}$ and $Re_{x,m}$ in table 1. The value of $Re_{x,c} = 3{\cdot}2 \times 10^5$ for $S = 0$ in figure 6 was obtained as follows. In the case of a non-rotating cone ($S = 0$), the perturbation equation of the present stability theory is reduced to the Orr–Sommerfeld equation. In that case it is known (Stuart 1963) that the critical Reynolds number obtained from the Orr–Sommerfeld equation relates closely to the shape parameter H of boundary layers. Because $H = 2{\cdot}56$ at $S = 0$ for the 30° cone, we have taken $Re_c = 545$ (based on displacement thickness) from Stuart (1963), which corresponds to $Re_{x,c} = 3{\cdot}2 \times 10^5$.

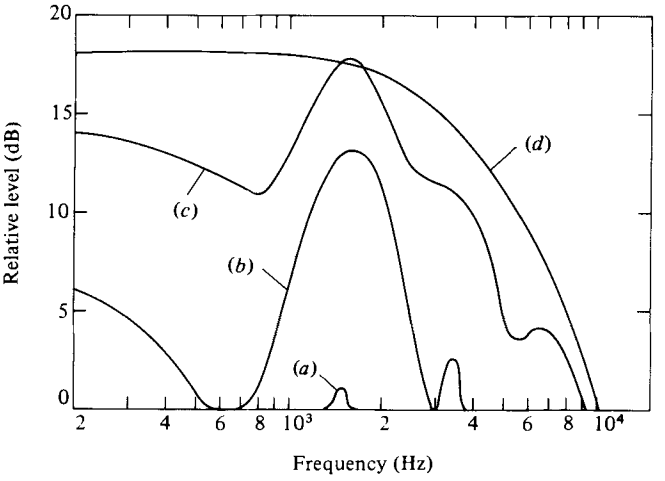

FIGURE 7. Frequency spectra of velocity fluctuations in transition region: (*a*) $S = 2{\cdot}01$, $Re_x = 2{\cdot}18 \times 10^4$; (*b*) 2·44, $2{\cdot}67 \times 10^4$; (*c*) 2·66, $2{\cdot}92 \times 10^4$; (*d*) 3·50, $3{\cdot}94 \times 10^4$.

Generally speaking, it should be noted that measured results for the critical Reynolds number $Re_{x,c}$ for instability might be dependent on the sensitivity of measuring instruments and the techniques used. Because the values of $Re_{x,c}$ measured in the present experiment were to be compared with the aforementioned linear instability analysis, careful measurements were made by using the hot-wire probe and a frequency analyser. Figure 7 shows frequency spectra of velocity fluctuations in the transition region. As shown with curve (*a*), the critical point $\tilde{x}_c$ was determined as the point where periodic signals obtained from the hot-wire probe were detected not by an oscilloscope but on the frequency spectrum. The corresponding values of $Re_{x,c}$ measured by the hot-wire probe coincided with those measured by the flow-visualization technique. Since a determination of the transition point $\tilde{x}_t$ by use of the oscilloscope was also indefinite, the transition point $\tilde{x}_t$ was defined here as the point where velocity fluctuations gave a frequency spectrum for the turbulent boundary layer as shown with curve (*d*) in figure 7.

It can be seen from figure 3(*b*) that the transition from laminar to turbulent flow on the rotating cone occurs not suddenly at a certain point but in a wide region of the cone surface. An example for $U_\infty = 3{\cdot}66$ m/s and $N = 2934$ r.p.m. indicated $\tilde{x}_c = 76$ mm for the critical point and $\tilde{x}_t = 154$ mm for the transition point, so that the length $\tilde{x}_t - \tilde{x}_c$ of the transition region was 78 mm. As shown in figure 6, the experimental values of the critical Reynolds number decreases with increasing rotational speed ratio S, which is the same trend as predicted by the theoretical analysis. There is, however, a quantitative difference between the experiment and the theoretical analysis. The experimental values of $Re_{x,c}$ are rather close to the theoretical Reynolds number $Re_{x,m}$ for maximum amplification.

In order to consider the difference of the critical Reynolds number $R_{x,c}$ between the theory and the experiment, velocity distributions in the laminar boundary layer were measured for $S = 0{\cdot}78$, 1·12 and 1·67, and are compared with the theoretical results for $S = 1$ and 2 in figure 8. As the displacement thickness δ_1 of the laminar boundary layers was as small as about 0·5 mm in the experiment, the accuracy of the velocity distributions measured was not sufficient. It could be said that there is no considerable difference between the theory and the experiment for the laminar velocity distributions.

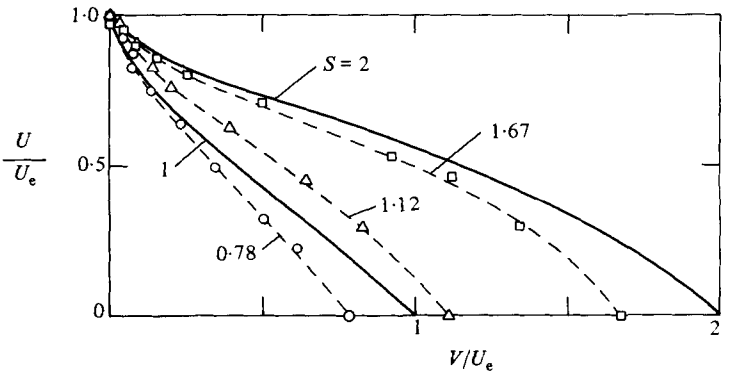

FIGURE 8. Velocity distributions in laminar boundary layers: ——, theory; – – – –, experiment.

As is well known, theoretical values of critical Reynolds number for instability of two-dimensional boundary layers are considerably lower than experimental values measured for natural disturbances, especially in a state of external low-turbulence flow, while, for centrifugal instabilities such as Taylor instability, critical values obtained from linear stability analyses are comparatively consistent with experiments. In the case of $S = 0$, the present problem corresponds to the former instability, while in the case of large S it includes a strong centrifugal instability. As seen in figure 6, the difference in the critical Reynolds number $Re_{x,c}$ between the theory and the experiment tends to become smaller as the local rotational speed ratio S is increased. It should also be noticed that the present experiment was made in flows of low turbulence.

Salzberg & Kezios (1965) measured the transition Reynolds number $Re_{x,t}$ $(= U_e\tilde{x}_t/\nu)$ by experiments on local mass transfer from a rotating 30° naphthalene cone of $2R_b = 68$ mm, and formulated it in relation to their rotational parameter $\omega R_b/U_\infty$ as

$$Re_{x,t} = 110960\left\{0{\cdot}73\left(\frac{\omega R_b}{U_\infty}\right)^{-2} + 0{\cdot}08\left(\frac{\omega R_b}{U_\infty}\right)^{-1}\right\}^{\frac{6}{7}}. \tag{2}$$

The transition point $\tilde{x}_t$ was determined from a deformation of the naphthalene surface due to mass transfer. In figure 9 this relation is compared with the present experiment by using the rotational parameter $\omega R_b/U_\infty$, because it is difficult to express their fomula (2) using the parameters in figure 6. Salzberg & Kezios' results are rather close to the present critical Reynolds number. Turbulence intensities in their experiment are not known. As indicated in Kobayashi (1981), it seems to be reasonable that the local critical Reynolds number $Re_{x,c}$ should be related not to the rotational parameter $\omega R_b/U_\infty$ but to the local rotational speed ratio $S(= \omega R/U_e)$. Okamoto *et al.* (1976) said from their experiment that the laminar–turbulent transition depends on the velocity ratio $\omega R/U_\infty$ and that the velocity ratio indicating the transition point was about 1·45 for the 30° cone.

3.4. *Measurements of the spiral vortices*

Two methods have been used in order to measure the direction ϵ of the axis of the spiral vortices. The first method is that using the parallel probe mentioned in §3.1, and the second one is direct measurement from many photographs obtained by the flow visualization. The results are given in figure 10. Both values measured by the

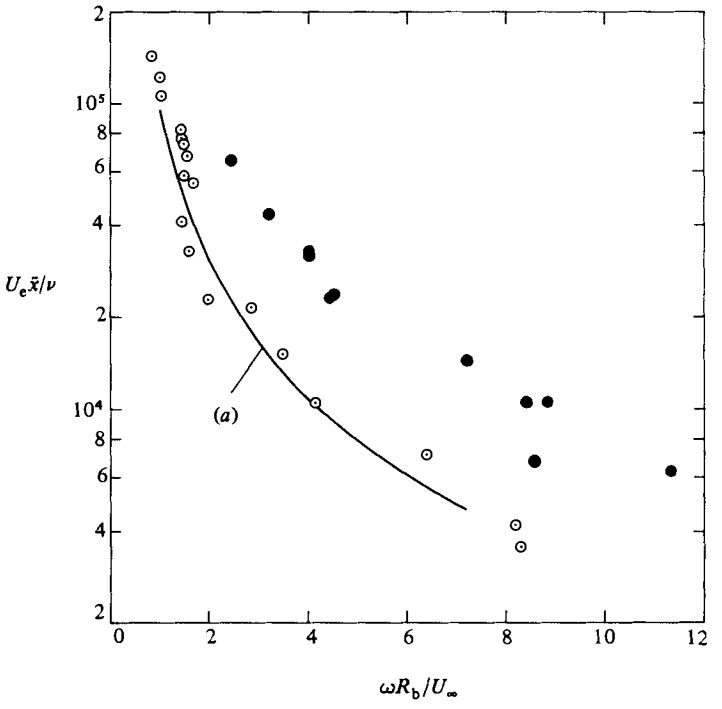

FIGURE 9. Comparison of the present experiment with Salzberg & Kezios' experiment (curve (*a*)). Present experiment: ○, critical; ●, transition.

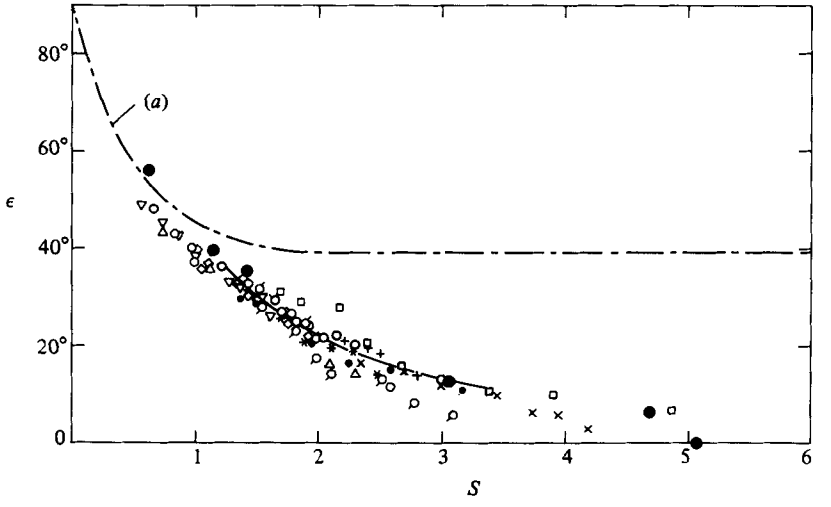

FIGURE 10. Angle ϵ of spiral vortices in relation to rotational speed ratio S. ●, hot wire; the other symbols were measured by flow visualization. Curve (*a*) is the direction of wall shear stress.

abovementioned two methods agree well. The appearances of the spiral vortices were more fluctuating than uncertainty intervals ($\pm 1{\cdot}0°$) for measurements of ϵ by both of the methods. The curve (*a*) in figure 10 is the theoretical direction of the wall shear stress in the laminar boundary layer, which is drawn for the purpose of comparison. It is clear that the angle ϵ measured by the flow-visualization technique differs from

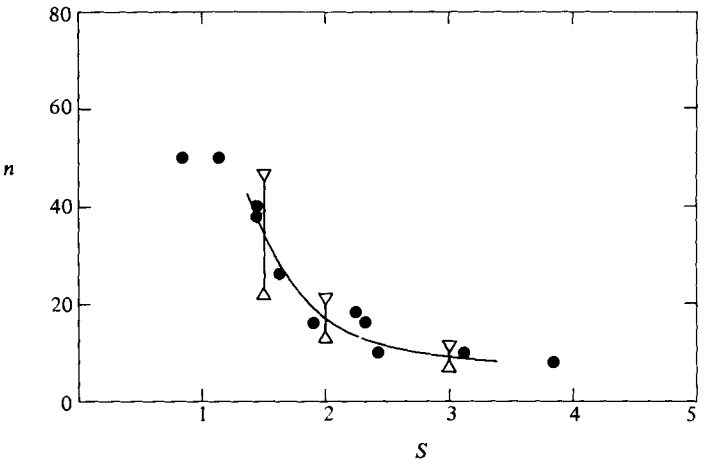

FIGURE 11. Number n of spiral vortices in relation to rotational speed ratio S: ●, experiment; △, theory using σ_c; ▽, theory using σ_m.

the direction of the wall shear stress. In figure 10 the same symbols for the flow visualization are given for a measurement along a meridian of the cone in one photograph. Figure 10 shows that the direction ϵ of the spiral vortices decreases as the rotational speed ratio S is increased, and that the theoretical values of ϵ shown by the solid line agree well with the experimental ones. When one examines the same symbols, one can find that the direction ϵ of each spiral vortex somewhat decreases downstream. This behaviour is similar to that for the rotating disk in still fluid, in which case the ϵ-value of spiral vortices decreases downstream from 14° to 7° (Kobayashi *et al.* 1980). As is found in figure 10, the angle ϵ becomes zero when the parameter S increases above about 5. It means that the spiral vortices change into the so-called Taylor vortices like piled doughnuts. We are interested in the fact that the spiral angle ϵ becomes zero not as $S \to \infty$ but at a finite S-value, because it is known for spiral flows between rotating cylinders (Schwarz, Springett & Donnelly 1964) that an axisymmetric mode of instability changes into a spiral mode at a certain axial flow velocity as the velocity is increased from zero.

Figure 11 shows the number n of spiral vortices appearing on the rotating cone, which was obtained from the photographs for different values of the approaching flow velocity U_∞ and the rotation speed N. Because the back side of the cone was invisible on those photographs, the uncertainty interval of n measured is estimated to be $\pm 5\,\%$. The figure indicates that the number n of spiral vortices decreases as the rotational speed ratio S increases. The prediction of n can be made by use of the relation $n = \sigma \sin\epsilon (Re_x \sin\theta)^{\frac{1}{2}}/\bar{\delta}_1$. If one adopts the theoretical values of σ_c, σ_m and ϵ in table 1 and the experimental critical Reynolds number $Re_{x,c}$ from figure 6, one obtains two values of n for each S, as shown in figure 11. The solid curve is drawn through their mean values. It can be said that the prediction of n is close to the experimental data.

The work of Mueller *et al.* (1981) for a rotating cylinder, which appeared during the final stage of preparing the present paper, also showed a similar trend to figure 10. They said that an angle (presumably $90° - \epsilon$, although the definition is not shown) for the rotating cylinder was approximately equal to arctan S. In their case the number n of spiral vortices remains approximately constant regardless of S or Reynolds number. This is different from the result in figure 11 for the rotating cone.

It is especially interesting that they observed simultaneous appearance of Tollmien–Schlichting waves and spiral vortices in a transitional process, as we have not observed such a state for the rotating cone.

4. Conclusions

Theoretical and experimental studies were carried out for the instability and the structure of transition region of the three-dimensional boundary layer on a 30° cone rotating in external axial flow. The results are summarized as follows.

(i) The critical Reynolds number $Re_{x,c}$, the direction ϵ of the spiral vortex axis and the number n of spiral vortices were theoretically determined in relation to the local rotational speed ratio S on the basis of the linear stability theory.

(ii) It was confirmed by the experiment that the disturbances of spiral-vortex type, predicted in the stability theory, appear in the transition region.

(iii) The process of transition from the onset of the spiral vortices to the turbulent state was observed in detail by using the flow-visualization technique.

(iv) The critical Reynolds number $Re_{x,c}$ and the transition Reynolds number $Re_{x,t}$ decrease with increasing rotational speed ratio S as shown in figure 6. The theoretical relation of $Re_{x,c}$ to S is qualitatively consistent with the experiment. However, the theoretical analysis gave smaller values than the experimental ones.

(v) The direction ϵ of the spiral vortices decreases as the parameter S increases, as seen in figure 10. The theory agrees well with the experiment. The ϵ-value of each spiral vortex reduces downstream. When the parameter S is above about 5, the angle ϵ becomes zero, so that the spiral vortices change into Taylor vortices.

(vi) The number n of spiral vortices decreases as the parameter S increases, as seen in figure 11.

REFERENCES

Chin, D.-T. & Litt, M. 1972 An electrochemical study of flow instability on a rotating disk. *J. Fluid Mech.* **54**, 613–725.

Gregory, N., Stuart, J. T. & Walker, W. S. 1955 On the stability of three-dimensional boundary layers with application to the flow due to a rotating disk. *Phil. Trans. R. Soc. Lond.* **A248**, 155–199.

Illingworth, C. R. 1953 The laminar boundary layer of a rotating body of revolution. *Phil. Mag.* **44**, 389–403.

Ito, H. *et al.* 1980 The design and performance of the low-turbulence wind tunnel, Tohoku University (in Japanese). *Mem. Inst. High Speed Mech., Tohoku Univ.* **44**, 93–151.

Kappesser, R., Greif, R. & Cornet, I. 1973 Mass transfer to rotating cones. *Appl. Sci. Res.* **28**, 442–452.

Kobayashi, R. 1981 Linear stability theory of boundary layer along a cone rotating in axial flow. *Bull. Japan Soc. Mech. Engrs* **24**, 934–940.

Kobayashi, R., Kohama, Y. & Takamadate, Ch. 1980 Spiral vortices in boundary layer transition regime on a rotating disk. *Acta Mech.* **35**, 71–81.

Koh, J. C. Y. & Price, J. F. 1967 Non-similar boundary-layer heat transfer of a rotating cone in forced flow. *Trans. A.S.M.E.* C: *J. Heat Transfer* **89**, 139–145.

Koosinlin, M. L., Launder, B. E. & Sharma, B. J. 1974 Prediction of momentum, heat and mass transfer in swirling, turbulent boundary layers. *Trans. A.S.M.E.* C: *J. Heat Transfer* **96**, 204–209.

Kreith, F. 1966 Frictional drag and convective heat transfer of rotating cones in mixed and turbulent flow. *Proc. Heat Transfer and Fluid Mech. Inst.* (ed. M. A. Saad & J. A. Miller), pp. 29–43. Stanford University Press.

MUELLER, T. J., NELSON, R. C., KEGELMAN, J. T. & MORKOVIN, M. V. 1981 Smoke visualization of boundary-layer transition on a spinning axisymmetric body. *A.I.A.A. J.* **19**, 1607–1608.

OKAMOTO, T., YAGITA, M. & KAMIJIMA, Y. 1976 Experimental investigation on the boundary-layer flow over rotating cone-cylinder body in a uniform stream. *Bull. Japan Soc. Mech. Engrs* **19**, 930–937.

SALZBERG, F. & KEZIOS, S. P. 1965 Mass transfer from a rotating cone in axisymmetric flow. *Trans. A.S.M.E.* C: *J. Heat Transfer* **87**, 469–476.

SCHWARZ, K. W., SPRINGETT, B. E. & DONNELLY, R. J. 1964 Modes of instability in spiral flow between rotating cylinders. *J. Fluid Mech.* **20**, 281–289.

STUART, J. T. 1963 Hydrodynamic stability. In *Laminar Boundary Layers* (ed. L. Rosenhead), p. 543. Oxford University Press.

TIEN, C. L. & CAMPBELL, D. T. 1963 Heat and mass transfer from rotating cones, *J. Fluid Mech.* **17**, 105–112.

TIEN, C. L. & TSUJI, I. J. 1965 A theoretical analysis of laminar forced flow and heat transfer about a rotating cone. *Trans. A.S.M.E.* C: *J. Heat Transfer* **87**, 184–190.